

**SYNTHESIS AND CHARACTERIZATION OF BARIUM TITANIUM OXIDE
(BaTiO₃) AND CALCIUM COPPER TITANIUM OXIDE (CaCu₃Ti₄O₁₂)
PELLETS AND THIN FILMS**

YEOH CHEOW KEAT

UNIVERSITI SAINS MALAYSIA

2008

**SYNTHESIS AND CHARACTERIZATION OF BARIUM TITANIUM OXIDE
(BaTiO₃) AND CALCIUM COPPER TITANIUM OXIDE (CaCu₃Ti₄O₁₂)
PELLETS AND THIN FILMS**

by

YEOH CHEOW KEAT

**Thesis submitted in fulfilment of the
requirements for the degree
of Doctor of Philosophy**

MAY 2008

ACKNOWLEDGEMENTS

I would like to thank Prof. Zainal Arifin Ahmad for all the guidance, advice and help given throughout the course of this study. I am also very grateful for his encouragement during some very trying times.

I would also like to thank Dr. Sabar Derita Hutagalung for his contributions and very useful discussions. I am also very grateful to the School of Materials and Mineral Resources Engineering, the Dean and academic, administrative as well as technical staff for providing the facilities and technical support. I wish to thank Universiti Sains Malaysia for providing financial support through a Graduate Assistant Scheme.

Additionally I would like to express my appreciation towards all those who have helped greatly through these few years. I am indebted to Prof. Zainal Arifin Ahmad, Dr Sabar Derita Hutagalung and Mrs. Khatijah Yaacob for all their help, particularly in the difficult months I was without a scholarship. Dr. Srimala Sreekantan and Dr. Sunara Purdwadaria helped greatly and taught me a lot about the low temperature aqueous synthesis method, the effects of high temperature on the Pourbaix diagram as well as the application of impedance spectroscopy. Discussions with Mr. Lim Chee Eng from Syarikat Ceramech, Mrs. Fong Lee Lee and Mr. Shahrul Ami Zainal Abidin helped greatly in setting up the gas flow measurements and electromagnetic shielding. I am also very grateful to Mr. Ben Garbowski of Corning Glass, USA for providing free samples of the zero-alkali glass substrates used in these experiments because I simply could not afford them. I would also like to thank Ms. Noorkhashimah Yeop for simply being a friend and listening. I am also very grateful to all those who, for some reason, cannot be named here for helping provide some of the materials and non-material support that was essential towards completing the research.

Last, but not least, I would like to thank my wife and parents for their patience, sacrifices and understanding these past few years.

Thank you all.

Yeoh Cheow Keat

TABLE OF CONTENTS

	Page
ACKNOWLEDGEMENTS	ii
TABLE OF CONTENTS	iv
LIST OF TABLES	vii
LIST OF FIGURES	viii
LIST OF SYMBOLS	ix
LIST OF PUBLICATIONS AND SEMINARS	xv
ABSTRAK	xvi
ABSTRACT	xviii
CHAPTER ONE : INTRODUCTION	
1.0 Introduction	1
1.1 Fabrication of thin films	1
1.2 Materials studied	2
1.3 Research approach and methodology	2
1.3.1 Fabrication and characterization of bulk powders	4
1.3.2 Fabrication and characterization of the thin films	4
1.3.3 Dielectric characterization of the pellets and thin films	5
1.4 Research objectives	5
CHAPTER TWO : LITERATURE REVIEW	
2.0 Introduction	6
2.1 Fabrication of thin films	6
2.1.1 Preparation of chemical precursors	8
2.1.2 Deposition techniques and film formation	10
2.1.3 Applications of electronic thin films	14
2.1.4 Requirements for ink-jet printing thin films	15
2.2 Synthesis of BaTiO ₃ and CaCu ₃ Ti ₄ O ₁₂	16
2.2.1 Synthesis of BaTiO ₃	16
2.2.2 Synthesis of CaCu ₃ Ti ₄ O ₁₂	26
2.3 Dielectric properties of BaTiO ₃ and CaCu ₃ Ti ₄ O ₁₂	27
2.3.1 Dielectric properties of BaTiO ₃	27
2.3.2 Dielectric properties of CaCu ₃ Ti ₄ O ₁₂	35

2.3.2.1	Structural effects	36
2.3.2.2	Equivalent circuit models	41
2.3.3	Impedance spectroscopy of BaTiO ₃ and CaCu ₃ Ti ₄ O ₁₂	46
2.3.4	Dielectric properties of BaTiO ₃ and CaCu ₃ Ti ₄ O ₁₂ thin films	57

CHAPTER THREE : MATERIALS AND METHODS

3.0	Introduction	65
3.1	Preparation of solution	65
3.1.1	Effects of composition	66
3.1.2	Effects of pH	67
3.2	Ink-jet printing of BaTiO ₃ and CaCu ₃ Ti ₄ O ₁₂ thin films	67
3.3	Preparation of BaTiO ₃ and CaCu ₃ Ti ₄ O ₁₂ pellets	69
3.4	Dielectric characterization of the pellets and thin films	70

CHAPTER FOUR : RESULTS AND DISCUSSIONS

4.0	Introduction	74
4.1	Synthesis of bulk powders from aqueous solution	74
4.1.1	Synthesis of BaTiO ₃ powders from aqueous solutions	74
4.1.2	Synthesis of CaCu ₃ Ti ₄ O ₁₂ powders from aqueous solutions	83
4.2	Ink-jet printing of BaTiO ₃ and CaCu ₃ Ti ₄ O ₁₂ thin films	92
4.3	Dielectric characterization of bulk pellets and thin films	96
4.3.1	Dielectric characterization of BaTiO ₃	97
4.3.2	Dielectric characterization of CaCu ₃ Ti ₄ O ₁₂	107
4.3.3	Dielectric characterization of BaTiO ₃ -CaCu ₃ Ti ₄ O ₁₂ mixtures	119

CHAPTER FIVE : CONCLUSIONS AND RECOMMENDATION FOR FUTURE RESEARCH

5.1	Conclusions	135
5.2	Recommendation for future research	136

LIST OF TABLES

		Page
Table 3.1	The mixture ratios and the sample notations used.	73
Table 4.1	Relative amounts of excess TiO_2 estimated from XRD and XRF analysis.	81
Table 4.2	The amount (vol%) of excess TiO_2 and CuO as evaluated through Rietveld refinement compared against figures rationalized from XRF analysis.	89
Table 4.3	The change in resistivity of the separate elements in BaTiO_3 when oxygen was introduced in varying concentrations at $500\text{ }^\circ\text{C}$.	106
Table 4.4	The change in capacitance of the separate elements in BaTiO_3 when oxygen was introduced in varying concentrations at $500\text{ }^\circ\text{C}$.	107
Table 4.5	The change in resistivity of the separate elements in $\text{CaCu}_3\text{Ti}_4\text{O}_{12}$ when oxygen was introduced in varying concentrations at $500\text{ }^\circ\text{C}$.	117
Table 4.6	The change in capacitance of the grain boundary elements when oxygen was introduced in varying concentrations.	117

LIST OF FIGURES

		Page
Figure 1.1	A printed design attainable using ink-jet printing without step-by-step photolithography.	1
Figure 1.2	A flow chart showing the various stages in this study.	3
Figure 2.1	A copy of a figure in Edison's patent application (Edison, 1904).	6
Figure 2.2	An example of the steps in the chemical solution deposition of thin films (Schwartz et al., 2004)	8
Figure 2.3	Cracks in spin coated BaTiO ₃ thin films after drying at 100 °C and heat treatment at 550 °C.	13
Figure 2.4	Potential-pH diagrams for (a) Ba and (b) Ti (Pourbaix, 1966) showing the regions of solubility in aqueous solutions.	19
Figure 2.5	Potential-pH diagrams for (a) Ca and (b) Cu (Pourbaix, 1966) showing the regions of solubility in aqueous solutions.	27
Figure 2.6	The (a) perovskite crystal structure for BaTiO ₃ showing the relative positions of the Ti and O ions (b) before and (c) after displacement.	28
Figure 2.7	The (a) perovskite-like structure of CaCu ₃ Ti ₄ O ₁₂ . The (b) close-up shows the tilting of the TiO ₆ cage.	36
Figure 2.8	The arrangement of the two different regions in a Pan and Benders' model (Pan & Bender, 2005).	42
Figure 2.9	An equivalent circuit commonly used for electroceramics.	47
Figure 2.10	The series and parallel path in the brick layer model.	56
Figure 2.11	The equivalent circuit used by Wang, Y.P. and Tseng (1999).	59
Figure 3.1	An original print head (a) before and (b) after clogging by the precipitate.	68
Figure 3.2	An example of the neutralization curve obtained by titration.	69

Figure 3.3	Thermocouple temperature versus controller temperature for the furnace used in electrical characterization.	71
Figure 3.4	The geometric parameters used in calculating the capacitance of the thin films (Kidner, N.J. et al., 2006).	72
Figure 3.5	The interdigital electrode structure used in the experiments.	72
Figure 4.1	The different amounts of precipitates obtained at different solution pH.	75
Figure 4.2	The Ba:Ti ratio of the final precipitates as evaluated by XRF (a) when pH was varied from 1 to 13 in 2 pH increments and (b) when pH was maintained at pH 13 and the initial Ba salt additions were varied.	76
Figure 4.3	TG-DTA traces for samples prepared using (a) stoichiometric additions of Ba ions at pH 1, (b) Ba ion additions in stoichiometric ratios at pH 13, and (c) Ba ion additions 10 % in excess of the stoichiometric ratio at pH 13.	77
Figure 4.4	XRD traces of (a) as precipitated samples prepared with an extra 10 % Ba ion addition as well as calcined at 1000 °C samples prepared with (b) an extra 10 % Ba ion addition at pH 13, (c) stoichiometric additions of Ba ions at pH 13, and (d) stoichiometric additions of Ba ions at pH 1.	79
Figure 4.5	XRD traces of the BaTiO ₃ powders (a) as precipitated were cubic and (b) after calcination at 1000 °C were tetragonal.	82
Figure 4.6	The (a) grain structure of the sintered BaTiO ₃ samples, (b) after image processing. After counting the grains (c), the results were arranged in a histogram (d).	82
Figure 4.7	The different amounts of precipitates when solution pH was varied.	83
Figure 4.8	The Ca:Ti and Cu:Ti ratio of the final precipitates as evaluated by XRF (a) when pH was varied from 1 to 13 in 2 pH increments. At pH 13, the initial salt additions for (b) Ca, (c) Cu and (d) Ti were varied independently of each other.	84
Figure 4.9	The (a) DTA and (b) TGA curves for the samples when pH was varied.	86

Figure 4.10	XRD traces of samples with stoichiometric ion additions prepared at pH 13 (a) as precipitated without heat treatment, and (b) heated to 500 °C. Samples prepared at pH 9 and heat treated at 1000 °C showed (c) extra TiO ₂ peaks which reduced in height when (d) pH was increased to pH 13 and (e) when stoichiometric conditions were met.	87
Figure 4.11	(a) Samples (P9) showing the presence of excess TiO ₂ phases and Cu rich phases; (b) samples (P9/1.10) showed only the presence of the Cu rich phase. (c) At pH 13 (P13), TiO ₂ phases were not clearly visible, however, the Cu rich phase was still visible. (d) In samples close to the stoichiometric ratio, minimal Cu rich phase was observed at the grain boundaries of the samples (P13/0.90/1.10).	90
Figure 4.12	The (a) grain structure of the sintered CaCu ₃ Ti ₄ O ₁₂ samples, (b) after image processing. After counting the grains (c), the results were arranged in a histogram (d).	91
Figure 4.13	A minimum of 5 print and heat treat cycles were needed to obtain visually homogeneous BaTiO ₃ and CaCu ₃ Ti ₄ O ₁₂ films.	92
Figure 4.14	Only one spin-coat cycle is needed to obtain homogeneous films.	93
Figure 4.15	Very fine structures were seen from the edges of the printed islands for both (a) BaTiO ₃ and (b) CaCu ₃ Ti ₄ O ₁₂ .	93
Figure 4.16	XRD traces of the (a) BaTiO ₃ and (b) CaCu ₃ Ti ₄ O ₁₂ films show the films to be of low crystallinity. The line trace below the XRD traces in (a) and (b) represent the standard diffraction pattern for BaTiO ₃ (ICDD #50626) and CaCu ₃ Ti ₄ O ₁₂ (ICDD #210140) respectively.	94
Figure 4.17	The thickness of the (a) BaTiO ₃ and (b) CaCu ₃ Ti ₄ O ₁₂ films as observed from the SEM was approximately 2 μm. The insets show the same figures after image analysis to determine thickness and surface roughness.	96
Figure 4.18	Impedance complex plane plot for the BaTiO ₃ (a) pellets and (b) thin films. The inset shows the non-zero intercept at 100 °C and 500 °C.	98
Figure 4.19	Modulus spectroscopic representation for the BaTiO ₃ pellets. The insets show the non-coinciding complex impedance and modulus peaks.	99
Figure 4.20	The equivalent circuit chosen to approximate the BaTiO ₃ pellets.	100

Figure 4.21	Partial curve fitting of the BaTiO ₃ thin film to obtain R and C values.	100
Figure 4.22	An Arrhenius plot showing the reciprocal of the resistances for the BaTiO ₃ pellets and thin films.	101
Figure 4.23	A Curie-Weiss plot for the BaTiO ₃ (a) pellets and (b) thin films.	102
Figure 4.24	The (a) real part of the dielectric constant and (b) the dielectric loss of the BaTiO ₃ pellets. The insets show the relevant values at approximately 10 kHz.	105
Figure 4.25	The (a) real part of the dielectric constant and the (b) dielectric loss of the BaTiO ₃ thin films. The insets show the relevant values at approximately 10 kHz.	106
Figure 4.26	The (a) dielectric constant and the (b) loss tangent when pH values were varied. The insets show the relevant values at approximately 10 kHz.	108
Figure 4.27	The dielectric (a) constant and the (b) loss tangent for samples prepared with Cu salts less than or in excess of the stoichiometric ratio. The insets show the relevant values at approximately 10 kHz.	110
Figure 4.28	Impedance complex plane plot for the CaCu ₃ Ti ₄ O ₁₂ (a) pellets and (b) thin films. The inset shows the non-zero intercept of the graph at 100 °C and 500 °C.	112
Figure 4.29	Modulus spectroscopic representation of the CaCu ₃ Ti ₄ O ₁₂ pellets.	113
Figure 4.30	An Arrhenius plot showing the reciprocal of the resistances for the CaCu ₃ Ti ₄ O ₁₂ pellets and thin films.	113
Figure 4.31	A Curie-Weiss plot for the grain boundary element in CaCu ₃ Ti ₄ O ₁₂ (a) pellets and (b) thin films.	114
Figure 4.32	The (a) real part of the dielectric constant and the (b) dielectric loss of the CaCu ₃ Ti ₄ O ₁₂ pellets. The insets show the relevant values at approximately 10 kHz.	115
Figure 4.33	The (a) real part of the dielectric constant and the (b) dielectric loss for the CaCu ₃ Ti ₄ O ₁₂ thin films. The insets show the relevant values at approximately 10 kHz.	116
Figure 4.34	The (a) dielectric constant and the (b) dielectric loss for the CaCu ₃ Ti ₄ O ₁₂ pellets when O ₂ was introduced. The insets show relevant values at approximately 10 kHz.	118
Figure 4.35	The (a) dielectric constant and the (b) dielectric loss for the CaCu ₃ Ti ₄ O ₁₂ thin films when O ₂ was introduced. The insets show relevant values at approximately 10 kHz.	119

Figure 4.36	The (a) dielectric properties and (b) loss tangent of the 3B1C pellets. The insets show the relevant values at approximately 10 kHz.	120
Figure 4.37	The (a) dielectric properties and (b) loss tangent of the 2B2C pellets. The insets show the relevant values at approximately 10 kHz.	121
Figure 4.38	The (a) dielectric properties and (b) loss tangent of the 1B3C pellets. The insets show the relevant values at approximately 10 kHz.	122
Figure 4.39	The (a) dielectric properties and (b) loss tangent of the 3B1C thin films. The insets show the relevant values at approximately 10 kHz.	123
Figure 4.40	The (a) dielectric properties and (b) loss tangent of the 2B2C thin films. The insets show the relevant values at approximately 10 kHz.	124
Figure 4.41	The (a) dielectric properties and (b) loss tangent of the 1B3C thin films. The insets show the relevant values at approximately 10 kHz.	125
Figure 4.42	The dielectric constant ($f = 10$ kHz) in the (a) pellets and (b) thin films. An upper and lower limit was based on a serial and parallel arrangement of the constituents.	126
Figure 4.43	Micrographs of samples (a) 3B1C, (b) 2B2C and (c) 1B3C.	127
Figure 4.44	The (a) dielectric properties and (b) loss tangent of the 1B3C pellets when oxygen was introduced. The insets show the relevant values at 10 kHz.	128
Figure 4.45	The (a) dielectric properties and (b) loss tangent of the 2B2C pellets when oxygen was introduced. The insets show the relevant values at 10 kHz.	129
Figure 4.46	The (a) dielectric properties and (b) loss tangent of the 1B3C pellets when oxygen was introduced. The insets show the relevant values at 10 kHz.	130
Figure 4.47	The (a) dielectric properties and (b) loss tangent of the 3B1C thin films when oxygen was introduced. The insets show the relevant values at 10 kHz.	131
Figure 4.48	The (a) dielectric properties and (b) loss tangent of the 2B2C thin films when oxygen was introduced. The insets show the relevant values at 10 kHz.	132
Figure 4.49	The (a) dielectric properties and (b) loss tangent of the 1B3C thin films when oxygen was introduced. The insets show the relevant values at 10 kHz.	133

Figure 4.50 The dielectric constant ($f = 10$ kHz) in the (a) pellets and (b) thin films when oxygen was introduced. An upper and lower limit was based on a serial and parallel arrangement of the constituents.

134

LIST OF SYMBOLS

ϵ	dielectric constant
T	temperature
γ	diffusivity
$\tan \delta$	dielectric loss
e	electron charge
d_g	average grain size
ϕ	potential barrier height
b_e	bulk mobility of electrons
C	capacitance
RH	relative humidity
V	volume
Z	impedance
Y	admittance
M	electric modulus
D	diffusion coefficient
R	resistance
ρ	resistivity
k	Boltzmann's constant
E_a	activation energy

LIST OF PUBLICATIONS & SEMINARS

1. Yeoh, C. K., Sreekantan, S., Hutagalung, S. D., & Ahmad, Z. A. (2007). Fabrication of BaTiO₃ thin films through ink-jet printing of TiO₂ sol and soluble Ba salts. *Materials Letters*. **61(2007)**: 4536-4539.
2. Yeoh, C. K., Ahmad, M. F., & Ahmad, Z. A. (2006). Effects of Cu and Ti excess on the dielectric properties of CaCu₃Ti₄O₁₂ prepared using a wet chemical method. *Journal of Alloys and Compounds*. **443(1-2)**: 155-160.
3. Yeoh, C. K., Sreekantan, S., Hutagalung, S. D., & Ahmad, Z. A. (2006). Microstructure of CaCu₃Ti₄O₁₂ prepared through a wet chemical method. Proceedings of the 15th Scientific Conference of the Electron Microscopy Society of Malaysia. Terengganu, Malaysia, December, 2006.
4. Yeoh, C. K., Sreekantan, S., Hutagalung, S. D., & Ahmad, Z. A. (2006). Inkjet printing of BaTiO₃ thin films from aqueous solutions. International Conference on X-ray and Related Techniques in Research and Industry (ICXRI 2006). Putrajaya, Malaysia, November, 2006.
5. Yeoh, C. K., Sreekantan, S., Hutagalung, S. D., & Ahmad, Z. A. (2005). Inkjet printing of CaCu₃Ti₄O₁₂ films. Proceedings of the 14th Scientific Conference of the Electron Microscopy Society of Malaysia. Penang, Malaysia, December, 2005.

SINTESIS DAN PENCIRIAN PELET DAN FILEM NIPIS BARIUM TITANIUM OKSIDA (BaTiO_3) DAN KALSIMUM KUPRUM TITANIUM OKSIDA ($\text{CaCu}_3\text{Ti}_4\text{O}_{12}$)

ABSTRAK

BaTiO_3 dan $\text{CaCu}_3\text{Ti}_4\text{O}_{12}$ ialah bahan seramik dengan pemalar dielektrik yang tinggi. Pemalar dielektrik tinggi BaTiO_3 disebabkan perubahan feroelektrik manakala sebab untuk $\text{CaCu}_3\text{Ti}_4\text{O}_{12}$ belum jelas. Cetakan semburan dakwat (*ink-jet printing*) digunakan untuk menyediakan filem nipis. Kaedah sintesis akueus bersuhu rendah digunakan kerana larutan yang digunakan tidak mengandungi mendakan. Serbuk, yang kemudiannya dibentuk menjadi pelet, dimendakkan daripada larutan dengan mengubah pH. Filem nipis diperoleh dengan mencetak larutan yang disediakan ke atas substrat kaca Corning 1737. Sekurang-kurangnya 5 kali cetakan diperlukan untuk memperoleh filem nipis yang tidak terputus-putus dengan ketebalan 2 μm . Tambahan awal Ba sebanyak 10% lebih daripada nisbah stoikiometri dan larutan pH13 diperlukan untuk mendakan BaTiO_3 stoikiometri. Untuk $\text{CaCu}_3\text{Ti}_4\text{O}_{12}$, 10% lebih Ca, 10% kurang Cu dan larutan pH13 diperlukan. XRD menunjukkan mendakan yang diperoleh mengandungi BaTiO_3 atau $\text{CaCu}_3\text{Ti}_4\text{O}_{12}$ dan <5% lebihan TiO_2 . Spektroskopi galangan (*impedance spectroscopy*) menunjukkan BaTiO_3 tidak homogen secara elektrik dan terdiri daripada tiga elemen elektrik: teras berkerintangan rendah, bahagian pukal feroelektrik, dan sempadan butiran berkapasitans tinggi. Hanya teras berkerintangan rendah dan sempadan butiran berkapasitans tinggi diperhatikan dalam $\text{CaCu}_3\text{Ti}_4\text{O}_{12}$. Tenaga pengaktifan, diukur daripada perubahan rintangan apabila suhu dinaikkan, hampir serupa untuk pelet dan filem nipis. Pelet BaTiO_3 menunjukkan sifat feroelektrik manakala filem nipis tidak. Pelet dan filem nipis $\text{CaCu}_3\text{Ti}_4\text{O}_{12}$ tidak menunjukkan sifat feroelektrik. Perubahan kecil dalam kapasitans dan rintangan diperhatikan apabila gas oksigen ditambah. Kapasitans untuk campuran BaTiO_3 - $\text{CaCu}_3\text{Ti}_4\text{O}_{12}$ berada di luar jangkaan model penyambungan siri dan selari mungkin disebabkan tindakbalas antara

BaTiO₃ dan CaCu₃Ti₄O₁₂. Pemalar dielektrik pelet (>2000) lebih tinggi berbanding filem nipis (<1000).

SYNTHESIS AND CHARACTERIZATION OF BARIUM TITANIUM OXIDE (BaTiO₃) AND CALCIUM COPPER TITANIUM OXIDE (CaCu₃Ti₄O₁₂) PELLETS AND THIN FILMS

ABSTRACT

BaTiO₃ and CaCu₃Ti₄O₁₂ are ceramic materials with high dielectric constants. However, the high dielectric constant in BaTiO₃ is due to a ferroelectric transition while the reason for CaCu₃Ti₄O₁₂ is not yet clear. Ink-jet printing was used to fabricate the thin films. The low temperature aqueous synthesis method was used because the solution form is precipitate-free. Powders, which were later shaped into pellets, were precipitated from the solution by varying pH. Thin films were obtained by printing out the solution on Corning 1737 glass substrates. At least 5 print cycles were required to obtain continuous 2 μm thick thin films. Initial Ba additions 10% in excess of stoichiometry and a pH13 solution was necessary to obtain stoichiometric BaTiO₃ precipitates. For CaCu₃Ti₄O₁₂, a 10% Ca excess, 10% Cu deficiency and a pH13 solution was necessary. XRD traces show precipitates were mainly BaTiO₃ or CaCu₃Ti₄O₁₂ with <5% excess TiO₂. Impedance spectroscopy shows the BaTiO₃ to be electrically inhomogeneous and made up of three different electrical elements: a low resistivity core, a ferroelectric bulk and a high capacitance grain boundary. Only the low resistivity core and high capacitance grain boundary was observed in the CaCu₃Ti₄O₁₂. Activation energies, measured from the change in resistance when temperature was increased, were almost similar for the pellets and thin films. The BaTiO₃ pellets showed ferroelectric behavior but the thin films did not. Both CaCu₃Ti₄O₁₂ pellets and thin films did not show ferroelectric behavior. Slight changes in the capacitance and resistance were observed when oxygen was introduced. The capacitances of BaTiO₃-CaCu₃Ti₄O₁₂ mixtures fell outside the prediction of serial and parallel connection models probably due to reaction between the BaTiO₃ and CaCu₃Ti₄O₁₂. The dielectric constant of the pellets (>2000) was higher than the thin films (<1000).

CHAPTER 1 INTRODUCTION

1.0 Introduction

One of the main drawbacks to widespread research and development of thin films is the high cost of fabrication. This thesis attempts to address this issue by using commonly available ink jet printers to fabricate thin films of BaTiO_3 and $\text{CaCu}_3\text{Ti}_4\text{O}_{12}$, two very high dielectric constant materials that have been widely researched. These thin films were then characterized.

1.1 Fabrication of thin films

Thin film fabrication methods may be broadly divided into physical and chemical methods. The physical methods have to be ruled out because they commonly employ very costly vacuum systems, leaving the chemical methods. Chemical methods typically involve solution deposition onto substrates. Lithography processes are then used to pattern the films. Using an ink jet printer bypasses the need for step-by-step lithography methods of patterning as the desired pattern may be printed directly unto the substrate (Figure 1.1). Although there have been custom built ink-jet systems for depositing ceramic inks, the costs for these are prohibitively high. This leaves the common desktop ink-jet printers that can be found in nearly every office worldwide.

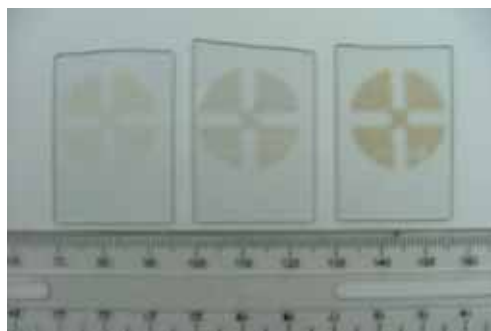


Figure 1.1: A printed design attainable using ink-jet printing without step-by-step photolithography.

The first part of this thesis concerns the preparation of suitable chemical solutions for printing thin films using a common ink-jet printer. A combination of microscopy, elemental spectroscopy and phase analysis was used to understand the synthesis process. The thin films are then heat treated and characterized using impedance spectroscopy. For purposes of comparison, the electrical properties of the pellets were measured as well to determine to what extent ink-jet printing has been able to duplicate the properties of the pellets.

1.2 Materials studied

BaTiO_3 and $\text{CaCu}_3\text{Ti}_4\text{O}_{12}$ are high dielectric constant materials of great interest for capacitive applications. Studies about the dielectric properties of $\text{CaCu}_3\text{Ti}_4\text{O}_{12}$ are relatively new compared to BaTiO_3 , hence the need to have BaTiO_3 as a main reference material. BaTiO_3 was chosen because of the considerable amount of information already available concerning its fabrication and properties. Historically, BaTiO_3 is one of the “classical” high dielectric constant materials developed during World War II (Haertling, 1999). On the other hand, although structural information about $\text{CaCu}_3\text{Ti}_4\text{O}_{12}$ has been known since the 1970s (Collomb et al., 1977), researchers have only begun to study and understand the dielectric properties (Ramirez et al., 2000; Subramanian et al., 2000). It is hoped that the knowledge gained from studying BaTiO_3 would help in understanding the fabrication and dielectric properties of $\text{CaCu}_3\text{Ti}_4\text{O}_{12}$.

1.3 Research approach and methodology

This thesis may be broadly divided into three parts (Figure 1.2): the fabrication of the powders, the fabrication of the thin films and the dielectric characterization.

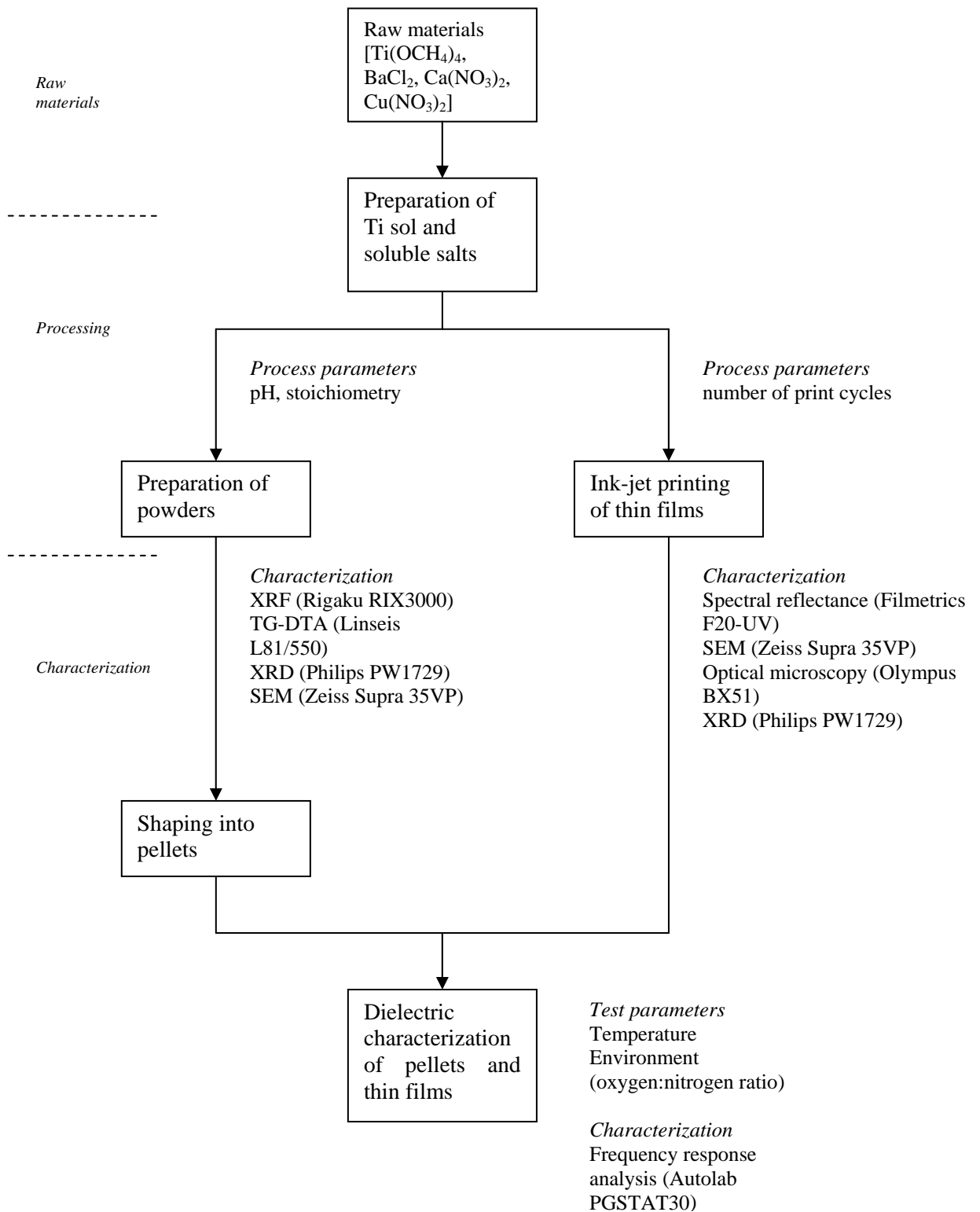


Figure 1.2: A flow chart showing the various stages in this study.

1.3.1 Fabrication and characterization of powders

The powders were fabricated starting from peptized TiO₂ sol, into which was added appropriate amounts of soluble Ba, Ca and/or Cu salts. The preparation of the pellets, in addition to providing a baseline for comparison, also helps in understanding the mechanism by which the compounds form. The powders were characterized using coupled Thermogravimetric and Differential Thermal Analysis (TG-DTA) to observe the stages in the compound formation. X-ray Fluorescence (XRF) analysis was used to determine the elemental composition of the compounds while X-ray Diffraction (XRD) was used to determine the phase content.

1.3.2 Fabrication and characterization of the thin films

The first requirement for the solution is that it must be able to be used in the ink-jet printer. Ink-jet printers have been used to synthesize everything from microcircuits to solar cell metallization to bulk ceramic components. The solution used must have very little or no suspended solids to avoid clogging the ink-jet dispenser. Ink-jet printers are increasingly capable of producing very fine droplets, with some manufacturers claiming picolitre droplets. Therefore, researchers are beginning to use sols, colloids or chemical solutions in place of the ceramic suspensions that have been used previously.

One of the “traditional” methods for producing sol-gel ceramics involves the hydrolysis and condensation of alkoxides. In recent years several other methods (Schwartz et al., 2004) have been advanced such as the metal-organic decomposition processes (Zhu et al., 2004) and the use of short chain carboxylates (Ohya et al., 2004) and other additions to adjust the form of the chemical chains. These different chains are useful in that they might be similar to the final compound and ease the formation of the compound. However, the chemistry is considerably more complex and

the type of reaction more difficult to predict. Therefore, to reduce the number of variables involved, the “traditional” alkoxide approach was selected. After printing, the thin films were characterized using optical and electron microscopy as well as spectral reflectance to determine the thickness and homogeneity of the films. XRD was also used to ensure phase formation in the thin films.

1.3.3 Dielectric characterization of the pellets and thin films

Dielectric characterization of the samples were carried out using impedance spectroscopy (also known as frequency response analysis). Dielectric characterization also helps to determine how successful the ink-jet printing was in replicating the properties of the pellets. During the measurement, temperature was varied from 100 °C to 500 °C in 100 °C intervals to determine the temperature dependence of the dielectric properties. At 500 °C, oxygen gas was introduced into a pure nitrogen testing atmosphere to determine the effects of different conditions on the dielectric properties.

1.4 Research objectives

The research objectives of this thesis are:

- i) To determine the process parameters (i.e. solution pH and initial stoichiometry) to obtain BaTiO_3 and $\text{CaCu}_3\text{Ti}_4\text{O}_{12}$ from a wet chemical process.
- ii) To fabricate homogeneous thin films of BaTiO_3 and $\text{CaCu}_3\text{Ti}_4\text{O}_{12}$ using a desktop inkjet printer.
- iii) To compare the effects of temperature and testing environment on the dielectric properties of the pellets and thin films.

CHAPTER 2 LITERATURE REVIEW

2.0 Introduction

The review will be focused initially on the requirements for the fabrication of thin films. The synthesis of the two materials used, BaTiO_3 and $\text{CaCu}_3\text{Ti}_4\text{O}_{12}$ are then discussed. Finally, the dielectric properties of BaTiO_3 and $\text{CaCu}_3\text{Ti}_4\text{O}_{12}$ are reviewed.

2.1 Fabrication of thin films

Thin films are usually less than a few microns in thickness (Stojanovic et al., 2002). However, the defined thickness is highly dependent on the target application (Schwartz et al., 2004). Historically, one of the pioneers of thin film technology was Thomas Edison (Edison, 1904) who had a patent for a vacuum bell jar-type apparatus to metallize objects (Figure 2.1). Since then many advances have been made, with thin films finding application in optical coatings, wear and corrosion resistant coatings, high temperature resistant coatings and even as electronic components. In electronics, the benefits of thin films over the bulk material include a faster response time, a smaller footprint and lower power requirements.

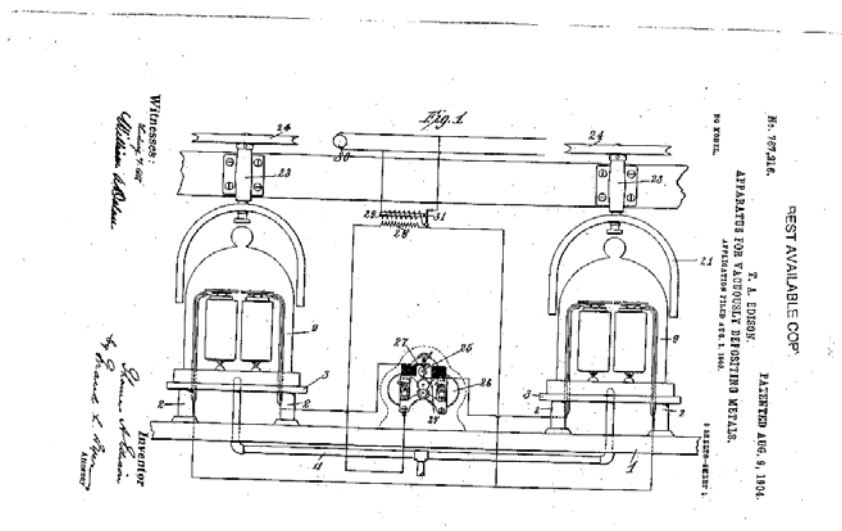


Figure 2.1: A copy of a figure in Edison's patent application (Edison, 1904).

In the production of thin films, it is important to have a controlled flux of material to the substrate so that a homogeneous film is produced. The various methods for producing thin films can generally be separated into physical and chemical methods (Sayer & Sreenivas, 1990). The physical methods usually use a solid of the compound or stoichiometric targets as the source material. An energy source is used to knock atoms out of the source material which is then deposited on the substrate. For example, sputtering uses an electron beam (Wang et al., 2002a), laser ablation uses a laser beam (Lopez et al., 2000; Lu et al., 2003; Miot et al., 1997), while thermal evaporation uses resistive heating as the energy source (Hwang & Souda, 2004). Advantages include compatibility with current semiconductor processes. Disadvantages include the amorphous nature of the deposited films which necessitate higher temperature deposition or post-deposition crystallizing processes (Halder et al., 2002). Line of sight deposition may cause non-uniformity if there is a step or topographic variations on the substrate.

The chemical methods are relatively cheaper because high vacuum systems are not required (Gust et al., 2001). A substrate is coated with a precursor solution which is dried to form a film (Figure 2.2). The required properties of the solution include solubility of the precursors without segregation, easily removed residues, lack of reaction with the substrate, and suitable rheology for deposition (Schwartz et al., 2004). Depending on the process, higher temperature crystallizing treatments may be required if the deposited films are amorphous.

The first well known instances of chemical solution deposition was probably the fabrication of SiO_2 or TiO_2 protective films on glass surfaces during the mid 20th century with electronic applications only being explored in the 1980s (Schwartz et al., 2004). Since this early work, "simple" oxides such as ZnO (Bukowski et al., 1997), BaTiO_3 (Phule & Risbud, 1989), SrTiO_3 (Jia et al., 1998) as well as complex solid

solutions/compounds such as $Ba_xSr_{1-x}TiO_3$ (Adikary & Chan, 2003), $SrBi_2Ta_2O_9$ (Ricote et al., 2004), $YBa_2Cu_3O_{7-\delta}$ (Sathyamurthy & Salama, 2000) and $Bi_{3.5}La_{0.5}Ti_3O_{12}$ (Zhu et al., 2001), have been fabricated. These methods usually result in thin films approximately 100 nm to 1 μ m in thickness although careful process control have resulted in thin films below 100 nm in thickness. Additionally, more viscous solutions have been used to produce films with thicknesses ranging in the tens of microns.

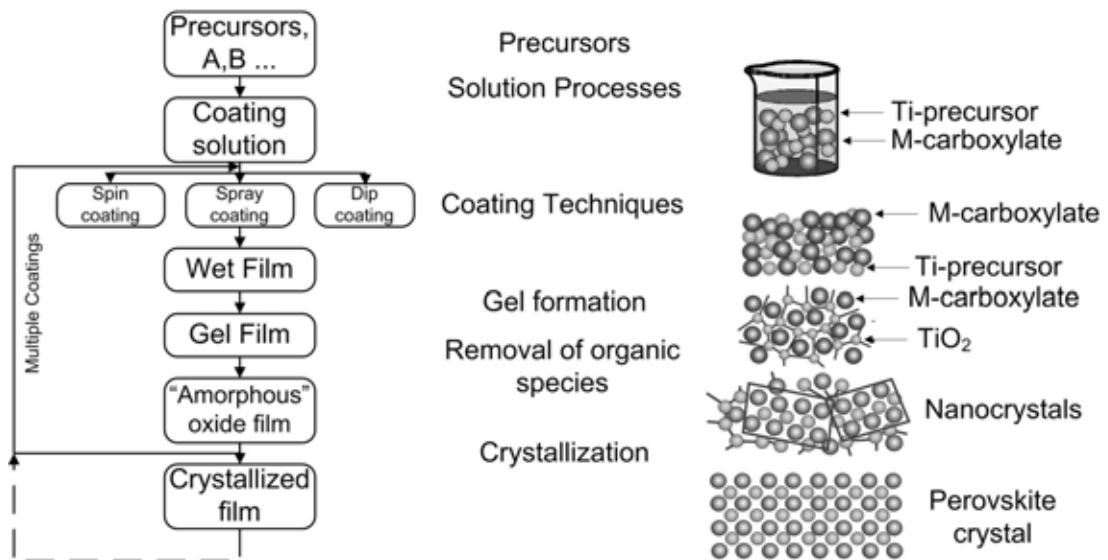
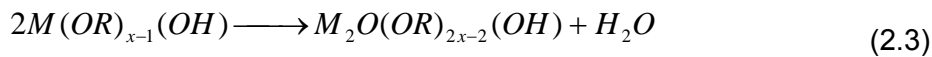
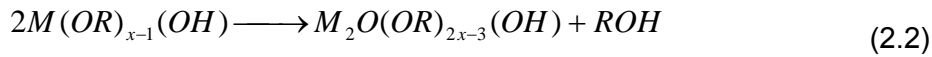
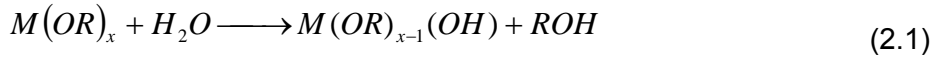


Figure 2.2: An example of the steps in the chemical solution deposition of thin films (Schwartz et al., 2004).

2.1.1 Preparation of chemical precursors

Sol gel methods were originally developed to make ceramics with unique and difficult to process compositions. Advantages of the sol gel techniques include low cost, high purity due to reduced contamination from grinding media, fine grain size, easier compositional control, and short fabrication cycle (Chatterjee et al., 2003; Ries et al., 2003). Sol-gel methods are probably not advantageous for the production of bulk powders because only relatively small quantities of powders are obtainable from large quantities of the solutions. However, the geometry of thin films with its large surface area and low volume is probably best suited for the sol gel process. Usually a

metallorganic compound or metal alkoxide is dissolved in suitable solvents (Zhang et al., 2002). The hydrolysis (Equation 2.1) and subsequent condensation (Equations 2.2 & 2.3) of this solution results in a gel complex or structured solution made up of long chains of metal-organic polymers.



Extensive, uncontrolled hydrolysis may lead to hydroxide formation which is undesirable if the final target is the formation of compounds (Schwartz et al., 2004). Controlled hydrolysis leads to the formation of short chains of polymeric species known as oligomers (Schwartz et al., 2004). This is usually accomplished via the addition of chelating agents (Bao et al., 1999) (e.g. ether linkages R-O-R', amine groups $-NH_2$, alcohol $-R-OH$ etc.) which stabilize the compound by forming extra linkages to the metal center of the alkoxide, hindering further complexation.

The "traditional" alkoxide process has undergone modifications to meet different process requirements while new techniques have been explored. For example, metal organic decomposition techniques (Zhu et al., 2004) involve dissolving metallo-organic compounds in suitable solvents. So-called hybrid processes utilize short chain carboxylates and alkoxides (Ohya et al., 2004). The resultant process, although not as chemically complex as the use of chelates (chelation, esterification, hydrolysis, polymerization), is more complex than the simple sol-gel processes (hydrolysis and condensation), thus limiting the control over the precursor structure. Diol and suspension processes (Arscott et al., 1997) are commonly used for thicker films obtainable through fewer deposition steps (approximately 1 - 2 μm per deposition step). This is accomplished by forming crosslinks between the chains thus creating

large oligomer molecules. These large oligomers as well as the non-gelling characteristic allow for thicker film deposits. In addition, the nitrate (Ng & Cima, 1997), citrate (Choy et al., 1998; Zhou et al., 2006) and Pechini (Fang et al., 2002) routes have also been used. In the nitrate routes, metal nitrates are dissolved in deionized water and alcohol before being deposited to form thin films. This method is straightforward without any complicated chemistry. However, drawbacks include the lack of substrate adhesion due to the absence of gelation. Also, the risk of recrystallization of the solid species as nitrates instead of the required oxides must also be addressed. The citrate solution process adds citric acid to the dissolved nitrates to chelate the solution. In the Pechini process, a polyhydroxyalcohol, typically ethylene glycol is added to the nitrate and citric acid solution to form organic ester compounds.

The “traditional” alkoxide route provides simpler chemistry and more predictable precursors compared to the various modifications which make it easier to adapt for ink-jet printing. Therefore, the emphasis from this point forward would be on the use of the traditional alkoxide process for the synthesis of the compounds.

2.1.2 Deposition techniques and film formation

The solution is deposited onto the substrate. After drying, the elemental constituents are held in very close spatial relation. This proximity is such that any chemical reaction is very much easier to initiate and complete, as in the use of very fine particulates in the solid state methods (Ando et al., 2004). The thickness of the film and properties dependent on solution viscosity may be adjusted by controlling the solution pH or type of solvent. On firing, the organic parts are decomposed and, subsequently, the remaining constituents oxidized to form the desired ceramic films. However, the structure of the ceramic films after firing is amorphous or partially crystallized and a subsequent annealing is required to fully crystallize the films.

Commonly used deposition techniques include spin coating, spray coating and dip coating. In spin coating, the substrate is affixed to a platform and flooded with the solution to be coated. The substrate is then spun at speeds between 1000 to 8000 rpms. Film thickness may be controlled by controlling the angular velocity, the solution viscosity, and the duration. Spray coating is accomplished by transforming the solution into an aerosol via an atomizer. The slow settling of the aerosol or electrostatic deposition may be employed. Dip coating only consists of immersing the substrate into the solution, slow withdrawal from the solution to form a film on the substrate and drying of the film. Film thickness is usually controlled by varying the solution concentration and the withdrawal speed. Another, less commonly used technique for ceramic thin films is electrochemical deposition (Guo et al., 2004; Lu et al., 2002; Wu & Lu, 2003).

In addition to these methods, tape casting is also used for processing thick films for multilayer ceramic capacitor applications. The ceramic particles are usually suspended within a polymeric binder to facilitate ease of fabrication (Yoon & Lee, 2004b). The resultant thick films must be subjected to high temperature treatment in order to burn out the polymeric binder.

Drying the film is important because as deposited films still contain a high amount of volatiles and organics. Depending on the precursors, the gelled films may be in the form of polymeric gels, physical aggregates of the polymeric chains or even non-gelling films (Schwartz et al., 2004). Fast heating is preferable to slow heating due to rapid collapse of the gel network before any blisters form (Schwartz et al., 2004).

Oxide or required compounds are usually obtained after heat treatment to remove the volatile organics. The possible types of reaction at this stage include pyrolysis, dehydration, or oxidation of the compounds (Schwartz et al., 2004).

Depending on the compound to be formed, the structure that is formed may help the formation of the desired compound, especially if it is almost similar. For example, in citrate solution combustion for producing $\text{Ba}_2\text{Ti}_9\text{O}_{20}$, the structurally similar Ti-O bonds helps in the formation of the compound during sintering (Zhou et al., 2006). Liu et al. (2005) have also observed the formation of intermediate compounds with similar structure to rutile, when they added sulfonic acid to their alkoxides after hydrolysis with the aim of obtaining nano-sized TiO_2 (rutile) particles. For the processing of BaTiO_3 films several steps are observed during heating (Schwartz et al., 2004). At temperatures between 300 – 350 °C, the titanium precursor decomposes to form a mixture of amorphous titanium oxide and crystalline titanium carboxylates. At temperatures between 400 – 500 °C, barium carboxylates are decomposed. Exact temperatures depend also on the precursor structures and bonds. Intermediate compounds such as $\text{Ba}_2\text{Ti}_2\text{O}_5\text{CO}_3$ might be formed as well which shifts the formation of BaTiO_3 to even higher temperatures (Duran et al., 2002; Shimooka & Kohiki, 1998). It has also been found that the use of nitrates result in crystalline oxides after combustion compared to the amorphous products from citrates (Zhou et al., 2006). This was believed to be caused by the nitrate precursors having a higher reactivity compared to the citrates, thus helping combustion to occur more completely while residual organics remained in the incompletely combusted samples. This also caused the samples prepared from nitrates to have higher densities than samples prepared from citrates (Zhou et al., 2006).

One of the problems with processing thin films is the high temperature (>600 °C) crystallizing heat treatments, which introduces residual thermal stresses within the thin films as well as the risk of diffusion from the substrate to the films. These residual stresses might lead to cracks (Figure 2.3). To overcome this, several processing methods, which involve lasers (Donohue & Todd, 2000) or rapid firing and annealing (Arscott et al., 1997), have been developed. Furthermore, using appropriate buffer

layers between the substrate and the thin films reduce considerably the thermal expansion mismatch (Lipinsky et al., 2005). Lopez et al. (2000) found that the pulsed laser deposited thin films they heat treated at 600 °C cracked due to the thermal expansion mismatch between the Pt substrates and the $\text{Ba}_{0.5}\text{Sr}_{0.5}\text{TiO}_3$. Other approaches for minimizing the cracks include the introduction of a glassy phase via boron doping of BaTiO_3 thin films (Yao & Zhu, 2002).

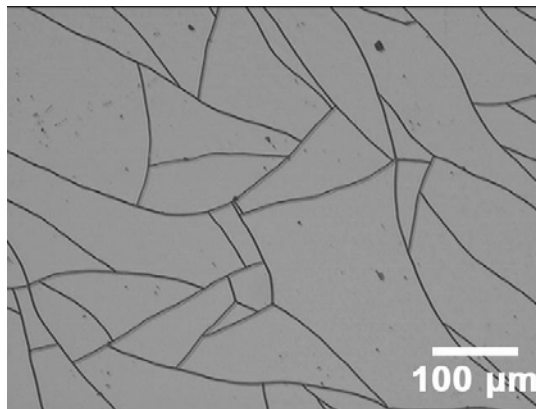


Figure 2.3: Cracks in spin coated BaTiO_3 thin films after drying at 100 °C and heat treatment at 550 °C.

Thin films may be amorphous/nanocrystalline (Krishna et al., 1997), polycrystalline (Xu et al., 1994), preferentially oriented (Jia et al., 1998) or, very rarely, single crystal structures (Saad et al., 2004). Different structures have different properties. For example, in capacitor applications the crystalline structures generally have higher dielectric constants than the amorphous structures (Xu et al., 1994). This might be due to the increase in tetragonality of the BaTiO_3 . Preferentially oriented or textured thin films may be better suited for some applications compared to other structures (Schwartz et al., 2004).

Since as-dried films are amorphous or very weakly crystalline, nucleation and growth processes determines the type of film structure that can be expected (Schwartz et al., 2004). Nucleation in the bulk of the film as well as the film-substrate interface

usually leads to polycrystalline thin films (Gust et al., 2001). The remaining organics or precursors influence the nucleation of new crystals and the final structure of the films (Schwartz et al., 1999). Epitaxial thin films develop through a small lattice mismatch between the substrate and the film (Peiying et al., 1995). For these films, the growth depends greatly upon nucleation at the film-substrate interface. The grains which grow from the interface gradually consume the small, randomly oriented grains in the film bulk.

For instance, rf-sputtered BaTiO₃ on Pt coated Si substrates exhibited greater crystallinity than uncoated Si substrates, probably due to the lattice mismatch between BaTiO₃ (a=0.3994 nm) and Si (a=0.3923 nm) (Wang et al., 2002a). However, this is the subject of some debate with some researchers believing this to be caused by the relative diffusion of Ba and Sr (Gust et al., 2001). These researchers believe that the final grain size in the thin films is the result two competing processes: the nucleation in the bulk and the nucleation at the substrate/thin film interface (Gust et al., 2001). Larger grains might be formed in thin films with extended high temperature treatment, due to the increased nucleation and grain growth. For films with repeated deposition and heating cycles to build up the thickness, grain growth at the substrate-thin film interface might be exaggerated because of the extended high temperature processing of the layers adjacent to the substrate (Gust et al., 2001).

2.1.3 Applications of electronic thin films

Ceramic thin films have found application in many electronic applications which would be very difficult to list completely. Lead zirconate titanate and barium titanate thin films have been studied as ultrasonic transducers (Du et al., 1999; Treu et al., 2004). In electroluminescent displays, lanthanum doped lead zirconate titanate (Sayer & Sreenivas, 1990) and barium titanate (Evangelou et al., 2000; Song et al., 1998) thin films with high breakdown strength and permittivity have been used to limit the amount

of DC current across the device. BaTiO₃ has also been studied as potential electrochemical or pH sensors (Wu & Lu, 2003). The gas sensing properties of zinc oxide has been studied (Shen et al., 2005). Ytria stabilized zirconia (Masumoto & Goto, 2004), strontium titanate (Zheng & Sorensen, 1999) and titanium oxide (Li & Chen, 1997) are used in potentiometric oxygen concentration cells or high temperature fuel cells by measuring the emf generated when the thin film is exposed to different oxygen partial pressures.

For capacitive applications, the dielectric constant is very important because it is this parameter that will determine the smallest component possible (Gust et al., 2001; Homes et al., 2003; Kyuho et al., 2002). Some believe that a size reduction is inversely proportional to the square of the relative permittivity (Fechine et al., 2006). The use of thin films also simplify the integration of capacitive elements thus reducing the need for discrete capacitors which take up a lot of space (Ramesh et al., 2003).

2.1.4 Requirements for ink-jet printing thin films

Ink jet printing has been shown to be a low cost alternative for the production of microcircuits (Sirringhaus et al., 2001; Teng & Vest, 1988b) or microlenses (Danzebrink & Aegerter, 1999) and for metallization of solar cells (Teng & Vest, 1987, 1988a), or even the fabrication of small structures such as micrometer-scale walls (Biehl et al., 1998; Guo et al., 2003; Mott & Evans, 2001; Noguera et al., 2005; Zhao et al., 2002). Researchers have also studied the use of ink jet printers for combinatorial research (taking an example from the pharmaceutical industry) with the aim of mining the periodic table for new ceramic compositions (Evans et al., 2001; Wang & Evans, 2005). The advantages of ink jet printing include the possibility of low cost, direct patterning without masking or selective etching (Seo & Lee, 2006), low wastage of materials and close control of the compositions (Ai et al., 2004). Recently, Shen et.al (2005) printed gas sensing ZnO thin films, showing the process to be a simpler, cost effective

processing route amenable to doping by Pd or similar composition variations (Kaydanova et al., 2003). BaTiO₃ films have also been printed on a commercial ink-jet using suspensions of the bulk powders (Ding et al., 2004). In ink-jet printing ceramic thin films, solutions with very fine or no suspended solids are needed (Hayes et al., 1999), therefore researchers have utilized very fine suspensions of ceramic particles (Lee & Derby, 2004; MacLaren & Ponton, 2000) and ink-jet systems custom built for delivering these suspensions (Ai et al., 2004). However, with the emergence of printers that deliver increasingly finer droplets, with some claiming picolitre droplets (de Heij et al., 2003; Gooray et al., 2002), it becomes more difficult to have increasingly finer particle suspensions. Therefore, several researchers have begun utilizing sols or colloids as their ceramic inks (Ding et al., 2003; Lewis, 2002).

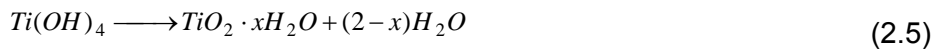
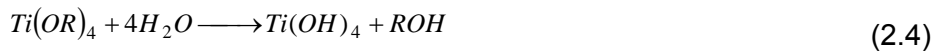
2.2 Synthesis of BaTiO₃ and CaCu₃Ti₄O₁₂

To summarize thus far, the “traditional” alkoxide process might be more suitable for ink-jet printing because of the relatively less complicated chemistry and the solid-free solution. This section focuses on the use of the “traditional” alkoxide process to synthesize BaTiO₃ and CaCu₃Ti₄O₁₂.

2.2.1 Synthesis of BaTiO₃

BaTiO₃ has been synthesized using a variety of methods including solid state methods, hydrothermal methods and low temperature aqueous methods (MacLaren & Ponton, 2000; Viviani et al., 2001; Viviani et al., 1999; Wada et al., 2001). The benefits of wet chemical synthesis include lower processing temperatures, more uniform grain sizes, higher purity and less risk of contamination by grinding media (Chatterjee et al., 2003; Ries et al., 2003). Since the wet chemical synthesis produces BaTiO₃ directly from the solution at relatively low temperatures, there is reduced risk of carbonation of unreacted Ba due to high temperature heat treatment (Kong et al., 2002; Ries et al., 2003). Solid state reactions typically require temperatures of approximately 1000 °C

(some researchers suggest 1150 °C) with higher temperatures necessary for dopants with low diffusivity values (Feteira et al., 2004). In addition, some researchers have noted that the wet chemical method allows for a higher dopant content without the formation of secondary phases compared to solid state methods (Hu et al., 2002). The low temperature aqueous method might hold the greatest promise for ink-jet printing because of the lower processing temperatures and the atmospheric pressure operating conditions. Low temperature aqueous synthesis usually starts from the preparation of a TiO₂ sol prepared from the hydrolysis and condensation of the titanium alkoxides (Qi et al., 2005; Vorkapic & Matsoukas, 1998) as shown in Equations 2.4 and 2.5.



The addition of acid provides an acidic media for the peptization. During peptization, primary particles and small clusters are removed from the large aggregates. In studying the effects of temperatures and alcohols on the size of the final TiO₂ nanoparticles, Vorkapic and Matsoukas (1998) found that the final size of the TiO₂ particles is determined ultimately by the peptization step. The size of the final particle is determined by the competing processes of peptization and reaggregation with high [H⁺]/[Ti] or low pH having a very high rate of peptization. They noted that the presence of residual alcohol, usually added to control the rate of growth during hydrolysis and condensation, promotes the reaggregation thus leading to larger final particles (Hwu et al., 2005). Therefore, it is very important to remove the excess alcohol before peptization. Moderate temperature increase promotes peptization by increasing the breakdown rates of the primary particle bonds. Excessive temperature increase has an adverse effect on the stability of the sol, decreasing the solvent dielectric constant and lowering the electrostatic barrier against reaggregation.

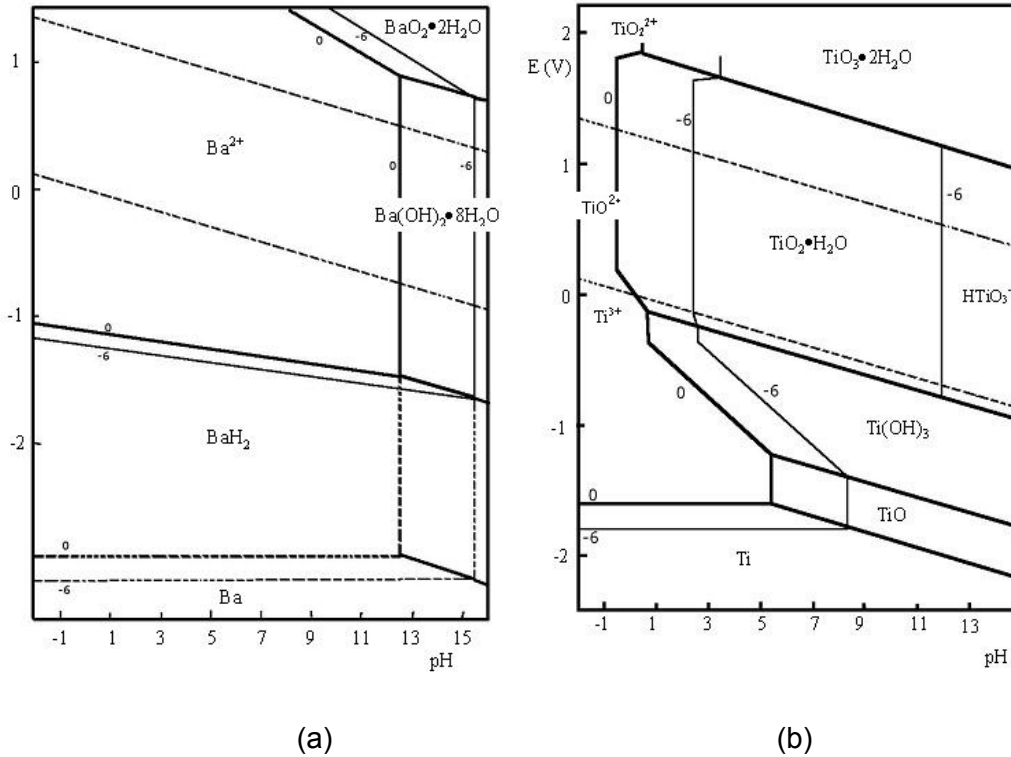


Figure 2.4: Potential-pH diagrams for (a) Ba and (b) Ti (Pourbaix, 1966) showing the regions of solubility in aqueous solutions.

Barium ions in the form of soluble salts are then added to the peptized solution. Due to the affinity of Ba for CO_2 , it is frequently necessary to purge the solution with an inert gas to reduce atmospheric CO_2 (Basca & Dougherty, 1995; Lu et al., 2000). In addition to forming carbonates, the excess CO_2 might react with the Ba and Ti to form intermediate phases which inhibit the crystallization of BaTiO_3 below $600\text{ }^\circ\text{C}$ (Gust et al., 2001). Several researchers have found that the amount of BaCO_3 present in commercial BaTiO_3 powders vary between 0.6-2.8 wt% (Yoon & Lee, 2004a). Although it is possible to remove the BaCO_3 through high temperature calcinations, it is not desirable to do so because of the higher cost. Several researchers have also found that heating in O_2 also can remove the BaCO_3 but results in lower surface areas and coarser particles (Demydov & Klabunde, 2004). The potential-pH diagram (Pourbaix, 1966) (Figure 2.4) shows that the Ti species is soluble in aqueous solutions at $\text{pH} < 3$, while Ba ions are soluble over a wide range of $\text{pH} < 13$. The differences in solubility

cause the leaching of Ba ions from BaTiO₃ particles suspended in aqueous solutions leaving a TiO₂ skin on the particles (BlancoLopez et al., 1997; Viviani et al., 1999). One of the methods used to overcome this via the addition of certain polyelectrolytes to passivate the surface of the BaTiO₃ particles. However, the drawback is certain salts, for example sodium salts (Wang et al., 2002b), may have detrimental effects on the electrical properties if left in the compound after the synthesis. A better choice might be the use of ammonium salts which are easier to remove via heat treatment (Shen et al., 2004).

Lower pH values frequently lead to the formation of other phases such as BaC₂O₄ and TiO(OH)₂ thus requiring higher calcination temperatures to decompose these compounds and form BaTiO₃. Increasing the pH value of the solution to pH 13 causes the precipitation of BaTiO₃ because it is the only stable phase under these conditions (Kim et al., 2003; Testino et al., 2004). Lowering the pH values of the aqueous solution after the BaTiO₃ has been formed usually does not completely cause dissociation into Ba(OH)₂ and TiO₂ but the leaching of Ba ions from the particle surface. This causes the formation of a non-water-permeable TiO₂ rich film over the TiO₂ particle that resists further dissolution (Urek & Drofenik, 1998).

Due to the limited solubility of TiO₂ and BaO in BaTiO₃ (<0.1 mol%) (Suzuki et al., 2001), an excess of any of these may lead to the formation of secondary phases such as Ba₆Ti₁₇O₄₀ (Bomlai et al., 2005) or Ba₂TiO₄. An excess of TiO₂ might lead to abnormal grain growth, due to the formation of a eutectic between BaTiO₃ and Ba₆Ti₁₇O₄₀ at 1332 °C (Lin & Lu, 2002; Proust et al., 1995; Rios et al., 1998) with increasing Ti excess leading to increasingly faceted grains (Cho et al., 2004). A slight excess of TiO₂ has been found advantageous in promoting lower sintering temperatures compared to the pure BaTiO₃ (Bomlai et al., 2005). The abnormal grain growth proceeds with increasing temperature with all the nucleation happening at the

beginning of the reaction. Rios et al. (1998) found experimental evidence that suggested the TiO_2 excess suppressed normal grain growth, while allowing for abnormal grain growth in several grains. Normal grain growth could be observed in barium excess samples (Cho et al., 2004). However, excess Ba could lead to the formation of large quantities of BaCO_3 after heating at $800\text{ }^\circ\text{C}$ or the barium rich Ba_2TiO_4 (Hennings et al., 2001).

Urek and Drofenik (1998) compared the use of $\text{Ba}(\text{OH})_2$ and $\text{Ba}(\text{CH}_3\text{COO})_2$ as Ba salt additions. Although using $\text{Ba}(\text{CH}_3\text{COO})_2$ resulted in samples with less BaCO_3 , decomposition products from the organic salt delayed the sintering time. These decomposition products usually record a peak in the TG-DTA curves with a corresponding weight loss at approximately $150\text{ }^\circ\text{C}$ to $600\text{ }^\circ\text{C}$. Some of the residual carbonized organic products which cannot be completely removed during washing of the powders are deposited on the surface of the BaTiO_3 grains and disintegrate during heating. Excess Ba may form Ba_2TiO_4 during sintering which may inhibit grain growth and degrade the microstructure (Proust et al., 1995; Urek & Drofenik, 1998). Some researchers (Drofenik et al., 2002) have noted that abnormal grain growth is not caused by Ba excess per se, but is more pronounced in the presence of other dopants such as SiO_2 or B_2O_3 . The BaTiO_3 reacts with the SiO_2 to form a liquid phase, BaSiTiO_5 , that helps the solution-dissolution process and aids the grain growth (Ueoka & Yodogawa, 1974). These dark blue abnormal grains, in addition to being more resistant to reoxidation, have semiconductive properties compared to the insulating normal light yellow grains. This led the authors (Drofenik et al., 2002) to speculate that oxygen expulsion during the abnormal grain growth is responsible.

There are two possible mechanisms (Eckert et al., 1996) for the formation of BaTiO_3 during wet chemical synthesis: a dissolution-precipitation mechanism and an in-situ mechanism. Hertl (1988) and other researchers (Kim et al., 2003; MacLaren &

Ponton, 2000) assumed an in-situ form of reaction where BaTiO₃ forms on the surface of the TiO₂ particle and proceeds through continued diffusion of the Ba ions inwards. They frequently point to the formation of a “raspberry-like” surface on the primary TiO₂ as proof of this (Kim et al., 2003). Pinceloup, et al. (1999) submitted what they believed to be evidence of the dissolution-precipitation mechanism when they used the hydrothermal method for the synthesis of BaTiO₃. They found smaller grain sizes when the solubility of the constituents was lowered because more particles nucleating at the same time ultimately lead to finer particles. In addition, completely amorphous or completely crystalline precipitates meant no BaTiO₃ crystallites were found on top of the amorphous TiO₂.xH₂O particles. Finally, fully reacted particles showed the presence of necks between them, which similar to those found in high temperature sintering, is more likely from a dissolution precipitation compared to an in-situ process. They argue that Ba ions found near the surface of the TiO₂ particles are only temporarily adsorbed and that the composition may still be considered as TiO₂.xH₂O. Furthermore, if an in-situ mechanism is involved, the size of the particle would be very close to the initial size of the TiO₂ from which the supply of Ti derives from. This was not observed with TiO₂ nanoparticles very much smaller than the BaTiO₃ particles (Pinceloup et al., 1999).

However, other researchers (MacLaren & Ponton, 2000) have observed after prolonged treatment of the precipitates, BaTiO₃ grew within and into the amorphous TiO₂. Researchers (Hertl, 1988; MacLaren & Ponton, 2000) seem to agree that the dissolution-precipitation mechanism is dominant during the early stages (i.e. nucleation) with the in-situ mechanism taking over in later stages (i.e. growth of the particle).

As precipitated BaTiO₃ particles prepared through wet chemical synthesis is generally cubic without the characteristic splitting of the (002) peak in its tetragonal

form (Feteira et al., 2004). In addition, the presence of any cubic phase may be observed as a cubic to tetragonal phase transition in DTA traces (Kim et al., 2003). The cubic structure is attributed to entrapment of hydroxyl ions within the perovskite lattice (Hennings et al., 2001; Pinceloup et al., 1999; Yan et al., 2005). Hennings et al. (2001) supported this observation using TGA and FTIR data. Although not being able to observe directly the entrapped ions, Qi et al. (2005) indirectly supported this argument with XRD peak broadening measurements that the lattice parameter of their barium strontium titanate nanoparticles were larger than the normal lattice. In addition, TG-DTA curves show weight loss without a corresponding endothermic/exothermic peak which the authors (Qi et al., 2005) attributed to the loss of the entrapped ions from the barium strontium titanate lattice. The lack of any clear endothermic/exothermic peak was believed to be caused by the already crystallized barium strontium titanate (Qi et al., 2005).

In the case of Sr additions, the XRD peak broadening might be due to the variation in lattice parameters of the SrTiO₃ solid solution (Bomlai et al., 2005). Some researchers also believe that the BaTiO₃ at room temperature is observed as a cubic or tetragonal structure depending on the size of the particles with particles below 0.07 μm being more likely to be observed as cubic through the absence of the XRD peaks splitting (Proust et al., 1995). However, this is also likely due to the broadening of the peaks for very small particles (Gust et al., 2001; Qi et al., 2005). This crystallite size factor is less evident after high temperature heat treatment (Bomlai et al., 2005). Other factors that may induce peak broadening include localized residual stresses that may be induced by deformation or surface grinding (Chen et al., 2005). High temperature heat treatment (>700 °C) is usually necessary for transformation to a more stable tetragonal form (Yan et al., 2005). The authors (Pinceloup et al., 1999) found the as precipitated powders to be Ba deficient even though XRD traces do not reveal extra phases other than BaTiO₃. Some researchers (Bocquet et al., 1999; Yan et al., 2005)

tried to address this problem by recrystallizing the precipitates under low temperature hydrothermal conditions. However, Jiang et al. (2000) in their research into very fine BaTiO₃ particles prepared from a stearic acid gel method, suggested that the cubic structure was not size related but rather a bulk property arising from the defects created during the stearic acid synthesis. Similar results were not observed for samples prepared using the more conventional alkoxide based sol-gel method. The crystals they prepared did not revert to the tetragonal form even after sintering at high temperatures (>1000 °C). Jhung et al. (2004) found cubic BaTiO₃ without the characteristic peak splitting in samples prepared from microwave irradiation and hydrothermal methods.

Lee et al. (2004) obtained tetragonal BaTiO₃ using a polymeric citrate precursor approach. The presence of Raman peaks indicating the presence of asymmetry within the TiO₆ octahedra was taken to mean that the BaTiO₃ was tetragonal. However, this measurement might not completely discount the presence of cubic phase in addition to the tetragonal BaTiO₃.

Choi et al. (1999) tried a microwave assisted hydrothermal method to overcome the problems with obtaining tetragonal BaTiO₃. They found Ba:Ti ratios of approximately 3 resulted in lower crystallinity compared with particles that were synthesized with particles closer to the stoichiometric ratio of BaTiO₃. They suggested that the excess Ba reacted with atmospheric CO₂ to form BaCO₃ seeds that promote further crystallization the BaTiO₃. They supported this supposition with XRD results which showed greater amounts of BaCO₃ for larger initial additions of Ba salts. However, for all their efforts, the degree of tetragonality for BaTiO₃ obtained through hydrothermal methods were largely unchanged. A further heat treatment at 250 °C was necessary to obtain tetragonal BaTiO₃.

Miot et al. (1995) found the BaTiO₃ they produced through a citric resin method to be a mixture of tetragonal and cubic phases as evaluated from the relative heights in the split of the (400) peaks. By assuming that the cubic phase is located at the surface of spherical tetragonal grains, they calculated the thickness of the cubic layer. They (Miot et al., 1995) also found the amount of cubic phase to decrease with increasing grain size. They believed higher dielectric constants in 1.6 μm grain size samples compared to 0.7 μm grain size samples could be caused by the higher presence of the cubic phase in the 0.7 μm sample which is unaffected by the ferroelectric transition.

Hirata et al. (1996) have found that hot isostatic pressing resulted in less porosity (< 10 %) compared to conventional pressureless sintering (30 – 40%) when powders with fine grain sizes were sintered at 950 °C and 1100 °C. However, the effect of this on the dielectric constant was not clear as the samples with higher densities had lower dielectric constants. Furthermore, the effects of porosity on the dielectric constant were almost non-existent for submicrometer sized grains. However, lowering the level of porosity was found to drastically reduce the dielectric loss. They also found that grain sizes below 0.4 μm generally led to cubic structures as revealed in XRD. The *c*-parameter increased with increasing grain size until maximum of approximately 3 μm when the *c/a* ratio was almost constant. They also observed a slight increase in the lattice parameters of the cubic BaTiO₃ for very fine grains. They found the dielectric constant to be greatly dominated by grain size with the maximum dielectric constant obtained when the grain size was approximately 1.4 μm.

Basca and Dougherty (1995) used a hydrothermal method to coat TiO₂ particles with a Ba rich solution thus forming a BaTiO₃ film on the particles. They used a similar approach to form BaTiO₃ films on Ti metal foils.